AD-A174 951 CARBON MONOXIDE AND TURBULENCE-CHEMISTRY INTERACTIONS MEASUREMENTS AND MO..(U) GENERAL ELECTRIC CO SCHENECTADY N Y RESEARCH AND DEVELOPMENT C..

1/1

UNCLASSIFIED S M CORREA 30 JUN 86 AFOSR-TR-86-2121 F/G 21/2 NL

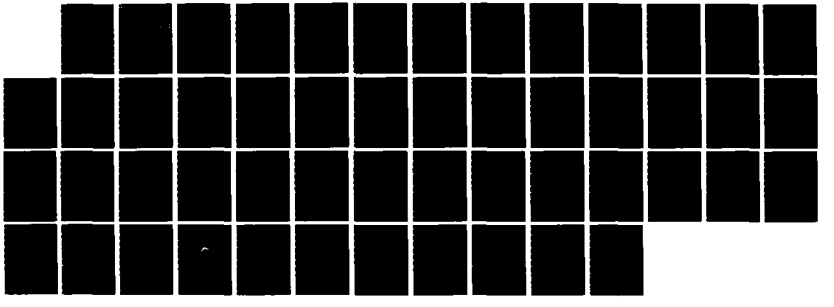

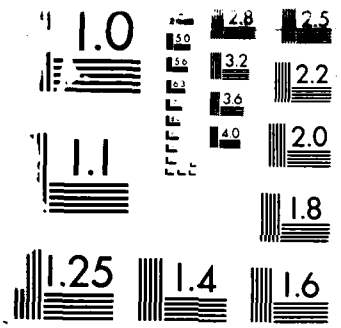
1.0
1.1
1.25
1.4
1.6
1.8
2.0
2.2
2.5
2.8
3.2
3.6
4.0

Unclassi
SECURITY CL

AD-A174 951

DOCUMENTATION PAGE

1a. REPORT: Unclassified	1b. RESTRICTIVE MARKINGS: None
2a. SECURITY CLASSIFICATION AUTHORITY	3. DISTRIBUTION/AVAILABILITY OF REPORT: Distribution unlimited; approved for public release
2b. DECLASSIFICATION/DOWNGRADING SCHEDULE	
4. PERFORMING ORGANIZATION REPORT NUMBER(S)	5. MONITORING ORGANIZATION REPORT NUMBER(S): AFOSR-TR- 86-2121
6a. NAME OF PERFORMING ORGANIZATION: General Electric Research and Development Center; 6b. OFFICE SYMBOL (If applicable)	7a. NAME OF MONITORING ORGANIZATION: Air Force Office of Scientific Research
6c. ADDRESS (City, State and ZIP Code): P. O. Box 8, Schenectady, New York 12301	7b. ADDRESS (City, State and ZIP Code): Bolling AFB DC 20332-6448
8a. NAME OF FUNDING/SPONSORING ORGANIZATION: Air Force Office of Sci. Res.; 8b. OFFICE SYMBOL (If applicable): AFOSR/NA	9. PROCUREMENT INSTRUMENT IDENTIFICATION NUMBER: F49620-85-C-0035
8c. ADDRESS (City, State and ZIP Code): Bolling AFB DC 20332-6448	10. SOURCE OF FUNDING NOS.

PROGRAM ELEMENT NO.	PROJECT NO.	TASK NO.	WORK UNIT NO.
61102F	2308	A2	

11. TITLE (Include Security Classification): Carbon Monoxide & Turbulence-Chemistry Interactions Measurements & Modeling of Turbulent Jet Diffusion Flames (unclassified)

12. PERSONAL AUTHOR(S): Dr. S. M. Correa

13a. TYPE OF REPORT	13b. TIME COVERED	14. DATE OF REPORT (Yr., Mo., Day)	15. PAGE COUNT
annual report	FROM 1 May 85 TO 1 June 86	June 30, 1986	32 + figures & tables

16. SUPPLEMENTARY NOTATION

17. COSATI CODES			18. SUBJECT TERMS (Continue on reverse if necessary and identify by block number)
FIELD	GROUP	SUB. GR.	Turbulence-chemistry interactions, extinction, blowoff, turbulent diffusion flames, superequilibrium, Laser diagnostics
21	01		
21	02		

19. ABSTRACT (Continue on reverse if necessary and identify by block number)

Development of a fundamental understanding of turbulence-chemistry interactions remains one of the most important and challenging problems in turbulent reacting flows. This program couples laser-based measurements and computer modeling of well-characterized laboratory-scale jet diffusion flames to study the effects of finite-rate chemistry and localized extinction in turbulent combustion. The long-range goal is to use this fundamental understanding for control of lean and high-altitude blow out in gas-turbine engines.

(over)

20. DISTRIBUTION/AVAILABILITY OF ABSTRACT	21. ABSTRACT SECURITY CLASSIFICATION
UNCLASSIFIED/UNLIMITED ☒ SAME AS RPT. ☐ OTIC USERS ☐	Unclassified

22a. NAME OF RESPONSIBLE INDIVIDUAL	22b. TELEPHONE NUMBER (Include Area Code)	22c. OFFICE SYMBOL
Julian M. Tishkoff	(202) 767-4935	AFOSR/NA

19. cont'd

The results of the first year of this program include: (1) improving the data base for $CO/H_2/N_2$ turbulent jet diffusion flames by analyzing direct measurements of CO_2 concentrations from Stokes vibrational Raman intensities and by comparing two independent methods of determining temperatures from the Raman data; (2) testing of the stretched laminar flamelet concept in turbulent diffusion flames by comparison of instantaneous and conditionally-averaged Raman measurements in turbulent H_2 and $CO/H_2/N_2$ jet diffusion flames with stretched laminar opposed-flow diffusion flame calculations and measurements; and (3) testing of a diffusion flame pilot for stabilization of turbulent jet flames at high Reynolds number.

CONTENTS

1. Summary

The results of the first year of this program include: (1) improving the data base for $CO/H_2/N_2$ turbulent jet diffusion flames by analyzing direct measurements of CO_2 concentrations from Stokes vibrational Raman intensities and by comparing two independent methods of determining temperatures from the Raman data; (2) testing of the stretched laminar flamelet concept in turbulent diffusion flames by comparison of instantaneous and conditionally-averaged Raman measurements in turbulent H_2 and $CO/H_2/N_2$ jet diffusion flames with stretched laminar opposed-flow diffusion flame calculations and measurements; and (3) testing of a diffusion flame pilot for stabilization of turbulent jet flames at high Reynolds number.

2. Research Objectives

The research objectives of this program are to:

A. Improve and expand the database for turbulent carbon monoxide/hydrogen/nitrogen jet flames utilizing pulsed Raman spectroscopic measurements.

B. Use experimental results to evaluate assumptions made in formulating prediction methods based on probability density functions and on laminar flamelets.

C. Modify the experimental facility to conduct turbulent jet combustion tests at Reynolds numbers greater than 9,000 without blow-off at nozzle. Use PLIF to visualize extent of extinction.

D. Model a carbon monoxide/hydrogen/nitrogen jet flame at 8,500 Reynolds number using two scalar and flamelet approaches.

E. Conduct experiments on two carbon monoxide/hydrogen/nitrogen jet flames at Reynolds numbers above 9,000 under conditions of local extinction.

F. Formulate alternatives to the partial-equilibrium chemical kinetics model previously used to predict the chemistry of carbon monoxide flames.

G. Extend laminar flamelet model for hydrocarbon flames.

3. Status

3.1 Introduction

Development of a fundamental understanding of turbulence-chemistry interactions remains one of the most important and challenging problems in turbulent combustion. This fundamental understanding of turbulent diffusion flames requires detailed knowledge of turbulent fuel/air mixing and combustion chemistry. None of these processes can be reliably calculated from rigorous fundamental theories. However, turbulent fuel/air mixing in simple nonreacting and reacting turbulent jet flows can be accounted for reasonably well using gradient diffusion models with assumed shape probability density functions (pdf's) of a conserved scalar, the mixture fraction. This model/experiment agreement occurs even though the turbulence model does not specifically account for the large-scale structures which may dominate the jet entrainment process. The reason may be that in round jets circumferential disturbances introduce instabilities which reduce or eliminate the coherence of large-scale structures, and thus diminish their significance. Concurrently, combustion chemistry (detailed mechanisms and reaction rates) is well established for the steady oxidation of H_2 and CO but becomes more complicated near extinction or for hydrocarbon fuels. Turbulence-chemistry interactions near extinction conditions are only beginning to be explored.

The approach of this joint experimental/computational program is to study turbulence-chemistry interactions in pilot-flame stabilized, turbulent, jet diffusion flames of H_2 and $CO/H_2/N_2$ fuels, where the turbulent fuel/air mixing and combustion chemistry are reasonably well known. Experimentally our unique combustor facilities and laser measurement techniques will be used to provide

time- and space-resolved measurements of probability density functions of velocity, temperature, major species concentrations, density, mixture fraction and OH concentration at various points in the flow along with two-dimensional images of OH concentration to provide qualitative extent of localized extinction. Measurements of local stretch (instantaneous gradient of compositional scalar) will also be attempted. Experimental results on stretched laminar opposed-flow diffusion flames are also available for comparison. Computationally, the single-scalar fast chemistry model with assumed shaped pdf, joint pdf models for scalar and dissipation rate closed with the laminar flamelet model,[5,8,41] and two- or three-scalar approaches using mixture fraction and extent of reaction variables will be developed. Detailed experiment-model comparisons will be used to assess models and to provide a more fundamental understanding of turbulence-chemistry interactions and extinction.

3.2 Turbulent Flame Facility: Prior Data

Laser diagnostic techniques of planar OH fluorescence, laser velocimetry, pulsed-Raman scattering, and laser-saturated OH fluorescence have been used in our laboratory to characterize turbulent jet-diffusion flames with H_2 and $CO/H_2/N_2$ fuels. The characteristics of the combustor and the initial conditions for the flames have been discussed in detail.[6,14,15,18,19,25] The combustor has a 3.2 mm internal diameter fuel tube centered axially in a 15-cm-square by 1-m long test section. The fuel velocity was controlled by calibrated critical flow orifices and the velocity of the surrounding co-flowing air stream by a servo-control on the exhaust fan. For the H_2 flames, the fuel jet had an initial average velocity of 285 m/s and is expected to have a turbulent pipe-flow profile corresponding to a cold-flow Reynolds number of 8500. The inlet air velocity was 12.5 m/s and was flat to within ±2%. The axial

pressure gradient (determined by 14 wall-pressure taps and by free-stream velocity measurements) was -51 Pa/m. For the $CO/H_2/N_2$ flame, the initial molar ratio of the fuel was approximately $40\%CO/30\%H_2/30\%N_2$ with a small amount of CH_4 (~ 0.7%) sometimes added. The initial fuel and air velocities were 54.6 m/s and 2.4 m/s, respectively, and were chosen to match the Reynolds number (8500) and initial fuel-to-air velocity ratio (22.8) of the H_2 flame. The initial jet velocity profile was measured 1 mm from the nozzle exit, and the axial pressure gradient was -1.0 Pa/m.

The experimental measurements on the turbulent H_2 flames are summarized elsewhere, particularly in References 14 and 19. The data include qualitative and quantitative imaging (Schlieren, shadowgraph, and planar OH fluorescence); instantaneous measurements of velocity (laser velocimetry); simultaneous measurements of temperature, density, individual major species concentrations, and mixture fraction (pulsed-Raman); and instantaneous measurements of OH concentrations (laser-saturated fluorescence). A collection of instantaneous measurements at a given flame location provide probability density functions (both conventional and Favre averaged). Analysis of those pdf's have permitted determination of intermittency and conditional moments.[36] The first four moments of the mixture fraction pdf show remarkable similarity to the moments measured in turbulent nonreacting jet flows and indicate the presence of broad mixing zones.[17] Comparison of the Raman data with thermodynamic and fluid mechanic models quantify the importance of preferential diffusion[13] of H_2 and of radical superequilibrium.[19] Superequilibrium was confirmed by direct measurements of OH concentrations using laser-saturated OH fluorescence with measured mean OH concentrations far above adiabatic equilibrium values close to the nozzle and near equilibrium values far downstream.[14]

The experimental measurements in the turbulent $CO/H_2/N_2$ flame are summarized in References 15, 6, and 18. The data include velocity, temperature, density, mixture fraction, and individual species concentrations as in the H_2 flame. In addition, probe sampling measurements of average value of NO and NO_x were obtained for the base fuel (for thermal NO_x), with small amounts of NH_3 added (for FBN conversion), and with small amounts of CH_4 added (for prompt NO_x).[18]

3.3 Calibration and Analysis of CO_2 Measurements

3.3.1 Objective

The goal in this portion of the work is to improve the data base for the turbulent $CO/H_2/N_2$ turbulent jet flames. Extensive data are available from our previous work on a turbulent jet diffusion flame with a molar fuel composition of $40\%CO/30\%H_2/30\%N_2$ with initial fuel and air velocities of 54.6m/s and 2.4m/s, respectively. These values were chosen to match the initial jet Reynolds number (8500) and initial fuel-to-air velocity ratio (22.8) of the previously characterized turbulent H_2 jet diffusion flame. The types of experimental data on this flame are summarized above. An ensemble of instantaneous measurements at a given flame location provides probability density functions and correlations.

The pulsed Raman measurements had one shortcoming. Although Stokes vibrational Raman scattering intensities from CO_2 were measured previously they were not analyzed because of the unknown fraction of the total CO_2 vibrational Raman profile which was in the experimental Raman bandpass. This fraction is expected to vary with temperature. The CO_2 mole fractions were determined previously by assuming that the total atomic carbon to hydrogen ratio

remained constant in the flame equal to the initial C/H ratio in the fuel. For example, $[X(CO_2) + X(CO)]/[X(H_2O) + X(H_2)] = 4/3$. Since the mole fractions of CO, H_2 and H_2O are known from their measured Stokes vibrational Raman scattering intensities, instantaneous mole fractions of CO_2 could be calculated. This approach was not totally satisfactory because (1) it ignores preferential diffusion effects which have been observed in turbulent H_2 jet diffusion flames and (2) it does not permit a totally independent measure of temperature from the sum of the mole fractions of all major species.

The purpose here is to report (1) the results of calibration experiments to determine the fraction of CO_2 Stokes vibrational Raman band which falls in the spectrometer bandpass as a function of temperature and (2) the reanalysis of turbulent $CO/H_2/N_2$ jet diffusion flame data.

3.3.2 Calibrations

A laminar, premixed porous plug burner was used for a series of calibration experiments. Temperatures were measured in the center of the flame one centimeter downstream from the burner in stoichiometric H_2 - air laminar flames with enough CO_2 added to the fuel to equal 30 mole percent in the burnt gas. Flame temperatures were independently controlled by inserting a series of stainless steel screens upstream of the measurement zone to increase the radiative heat loss. Figure 1 shows the comparison of temperature measurements with radiation-corrected silica-coated fine wire (0.176mm coated bead diameter) Pt/PtRh thermocouples with temperatures measured by pulsed Raman scattering using the N_2 Stoke/anti-Stokes ratio method. The results show excellent agreement--deviations are equal to the expected error in the Raman measurements (+50K).

Figure 2 shows the calculated apparent CO_2 mole fraction calculated from the measured CO_2 Stokes vibrational Raman intensity assuming that the percentage of CO_2 vibrational Raman band in the spectrometer bandpass is independent of temperature. Thus for the spectral bandpass used, the calculated apparent CO_2 mole fraction was constant from 300 to 1000K and then slowly increased with temperature. However, the total variation was less than 20% from 300-1700K.

3.3.3 Reanalysis of Turbulent Flame Data

Appropriate correction factors for CO_2 were added to the Raman data reduction program and the previous Raman data for the Re=8500 turbulent $CO/H_2/N_2$ jet diffusion flame were reanalyzed. The corrected data at X/d=10, 25 and 50 are listed in Tables I-III.

The most significant differences between the previous Raman calculations assuming a constant C/H ratio (RTCX Raman data reduction program) and the present Raman calculation (RLTC Raman data reduction program) are shown in Figure 3. The new calculations give larger values of CO_2 close to the center of the jet and smaller values of CO_2 on the edges. Similar trends are seen at X/d=10 and 50. This difference is likely the result of preferential diffusion of H_2 which rapidly diffuses from rich to lean zones. Assuming the carbon element diffuses with the hydrogen element would tend to underestimate CO_2 in lean zones (as observed in Figure 3). Much larger preferential diffusion effects have been experimentally observed with this fuel in laminar opposed-flow diffusion flames. Thus the present calibration experiments and data reanalysis have reduced one source of systematic error in pulsed Raman measurements in turbulent $CO/H_2/N_2$ jet flames.

3.4 Assessment of Laminar Flamelet Approach

3.4.1 Objective

The laminar flamelet model offers a physically appealing methodology for coupling complex chemistry with turbulent straining. This section provides a more quantitative test of the stretched laminar flamelet approach in H_2 and $CO/H_2/N_2$ turbulent jet diffusion flames by comparing <u>instantaneous</u> measurements of scalar variables using laser diagnostic techniques with laminar flamelet experiments or model calculations. Pulsed-Raman spectroscopy provides simultaneous measurements of temperature and concentrations of H_2, O_2, N_2, CO, CO_2, and H_2O with a spatial resolution of $<0.1\ mm^3$ and a temporal resolution of 2 μsec. These instantaneous measurements and conditionally averaged values are compared with stretched laminar flamelet calculations for H_2 flames[9] and stretched laminar-flame experiments for $CO/H_2/N_2$ laminar opposed-flow diffusion flames.[18] The latter experiments were supported by the Basic Research Department of the Gas Research Institute under Contract 5081-263-0600 (Mr. James Kezerle, Program Manager). Limitations of the laminar flamelet approach due to preferential diffusion and slow reactions (i.e., three-body recombinations or CO burnout) are discussed and the influences of localized extinctions are examined.

3.4.2 Background

It has been conjectured that turbulent jet-diffusion flames consist of laminar flamelets stretched and distorted by the turbulence.[5,8,41] This view has been supported qualitatively by a large number of experiments using probes (fast response thermocouples and ion probes) and line-of-sight images (Schlieren and shadowgraph) which demonstrate that reactions occur in highly localized positions in turbulent jet-diffusion flames. Only recently has this

view been substantiated directly through quantitative laser-induced OH fluorescence imaging of flamefronts in laminar, transitional, and turbulent H_2 jet-diffusion flames[16,19,25] and pilot-flame stabilized turbulent CH_4 flames.[10]

The laminar flamelet concept has also been proposed as a convenient approach for including detailed chemical kinetics in turbulent combustion models. It provides an alternative way of including finite-rate chemistry effects in turbulent combustion models.[35] The structures of turbulent and laminar flamelets are assumed to be the same, so the relationship between mixture fraction and species concentrations can be obtained from laminar diffusion-flame modeling or experiments. If the structure is assumed to be infinitesimally thin,[4] the laminar flamelet approach reduces to the equilibrium chemistry model mentioned earlier. If the structure is calculated assuming high energy asymptotics,[29] then the approach corresponds to a single step kinetics scheme. More often, experimental measurements in laminar diffusion-flames[2,21,23,32-34,38] are used. Bilger[2] has shown that the local temperature and concentrations of major species are given by the local mixture fractions, regardless of location in CH_4 counterflow laminar-diffusion flames of Tsuji and Yamaoki,[38] and similar results are obtained for a laminar CH_4 flame into still air.[32] However, Bilger[2] states that these concentration and temperature relationships with mixture fraction may not be universal and may depend upon the "stretching" of the flame. This dependence has been tested theoretically in laminar opposed-flow flames of methane[12,31] and experimentally[18] in laminar opposed-flow flames with $CO/H_2/N_2$, CO/H_2, and CH_4/N_2 fuels. Relationships of mixture fraction vs. major species mole fractions were found to be insensitive to variations in stretch (or scalar

dissipation X) over a wide range, but significant variations were observed near extinction.

Measured or calculated laminar flamelet or "stretched laminar flamelet" relationships have been used by Williams,[41] Marble and Broadwell,[30] Liew et al.,[27,28] Eickhoff and Grethe,[20] and Peters,[35] to model turbulent diffusion flames. One method of testing this approach has been to compare experimental time-averaged measurements of average temperature and molecular compositions vs. average mixture fraction (using thermocouples and probe sampling) in turbulent jet-diffusion flames of CO[37] and of hydrocarbons[20,23] with measurements or models of laminar-diffusion flames. Although reasonable agreement was claimed, there is no fundamental reason to believe that laminar flamelet relationships should be valid for conventional time-averaged measurements in turbulent diffusion flames with large fluctuations in instantaneous mixture fraction and flame stretch. The preferred methodology for assessing the laminar flamelet approach in turbulent jet-diffusion flames is to model these fluctuations and to compare the calculated average temperature, density and molecular compositions with those measured experimentally. This approach also leads to reasonable agreement,[20,28,30] but suffers from uncertainties in the fluid mixing model, in the assumed shape of the pdf's of ξ and X, and in the assumed relationship between ξ and X.

This section continues the analysis of Raman and laser-saturated fluorescence data by processing the data in ways in which it can be quantitatively compared with stretched laminar flamelet model calculations and experiments. In H_2 flames, simultaneous pulsed-Raman measurements of temperature and mixture fraction and of the H_2 and O_2 mole fractions are analyzed. In turbulent $CO/H_2/N_2$ flames, simultaneous Raman measurements of temperature and mixture

fraction and of the extent of H_2 conversion $[X(H_2O)/(X(H_2) + X(H_2O))]$ and CO conversion $[X(CO_2)/(X(CO) + X(CO_2))]$ vs. mixture fraction are presented. In each case, the Raman data are also averaged in narrow mixture fraction intervals. Conceptually, either instantaneous or conditionally averaged data should be comparable directly to stretched laminar-flame data. Time-averaged data at a fixed spatial location in turbulent diffusion flames correspond to a wide range of mixture fraction fluctuations and so may not be directly comparable with stretched laminar-flame data.

Experimental measurements of stretched laminar flames of H_2 are not available, but calculations using detailed chemical rate constants and molecular transport fluxes have recently appeared.[9] These laminar diffusion-flame calculations at two values of flame stretch (velocity gradients of 100 s^{-1} and 12,000 s^{-1}) are compared here with turbulent diffusion flame data. The higher value of flame stretch corresponds to a flame near the extinction limit.

Detailed experimental measurements of stretched laminar-diffusion flames of $CO/H_2/N_2$ fuel have recently been obtained in our laboratory using laser diagnostic and probe sampling techniques. Detailed measurements are presented elsewhere,[18] but some results are compared here with the turbulent flame data. The experimental values of flame stretch (a = 70, 180 and 330 s^{-1}) are believed to be far from the extinction limit, and the correlations of reactive scalars and mixture fractions were found to be relatively independent of a.

3.4.3 H_2 Flames

Pulsed-Raman data (approximately 30,000 data points) for the simultaneous measurement of temperature and mixture fraction in the Re = 8500 turbulent H_2 jet flame are shown in Figure 4. Each data point corresponds to a single

laser shot measurement (sample time <2 μs and sample volume <0.1 mm^3). The solid line in Figure 4 corresponds to calculated adiabatic equilibrium conditions for H_2-air mixtures. Close to the fuel nozzle (at x/d = 10) the experimental data show temperatures considerably above the adiabatic equilibrium curve in lean flame zones (mixture fraction <0.02). Near-stoichiometric (mixture fraction = 0.0283) and rich flame zones have temperatures considerably below the AE line. Near the center of the turbulent flame (x/d = 50), the Raman results are reasonably close to the AE line. Far downstream, past the time-averaged end of the turbulent flame (x/d = 200), all of the rich flame pockets have burned out and the measurements are in good agreement with the AE curve.

In order to more clearly show trends, the Raman data have been averaged in narrow mixture fraction intervals. Results are shown in Figure 5 for extensive Raman data at x/d = 10, 25, 50, 100, 150, and 200 in the turbulent H_2 jet-diffusion flame. The conditionally-averaged data demonstrate large deviations from AE close to the nozzle (x/d = 10 and 25) and progressively smaller deviations from AE further downstream. Also shown as dashed lines in Figure 5 are the calculations of laminar H_2 diffusion flames.[9] For the flame which is not highly stretched (a = 100 s^{-1}), the peak flame temperature is 2280 K—not much lower than the peak calculated AE temperature of 2380 K. The large calculated deviation from AE in fuel-lean regions of the laminar flame is attributed to preferential diffusion (David et al.[9]). This may also be the reason for the same deviations observed in fuel-lean regions of the turbulent flame at x/d = 10 and 25. This would indicate that preferential diffusion is much smaller in turbulent H_2 flames than in laminar H_2 flames.

Calculations for the very highly stretched laminar H_2 flame close to the extinction limit (α = 12,000 s^{-1}) show a peak flame temperature of only 1400 K. Figure 5 demonstrates that the present turbulent H_2 flame data (when conditionally averaged) is far from extinction. Comparing the calculated curves in Figure 5 with the instantaneous data in Figure 4 shows that even instantaneous flame zones are not stretched to extinction although some instantaneous measurements at x/d = 10 are close to it.

Another characteristic of highly stretched laminar flames is the overlap of fuel and air. Instantaneous Raman measurements of mole fractions of H_2 and O_2 near the nozzle (x/d = 10) of the turbulent H_2 flame are shown in Figure 6. The solid line in Figure 6 shows that very little overlap of H_2 and O_2 is expected at adiabatic equilibrium conditions (at most $X(H_2) = X(O_2) \sim 0.007$). The fuel-air overlap is calculated[9] to be much greater in stretched laminar-diffusion flames ($X(H_2) = X(O_2) \sim 0.025$ at α = 100 s^{-1} and $X(H_2) = X(O_2) \sim 0.075$ at α = 12,000 s^{-1}). The pulsed-Raman measurements from the turbulent H_2 flame in Figure 6 show substantial fuel-air overlap at this flame location close to the nozzle. In general, the turbulent flame data lie between the AE curve and α = 12,000 s^{-1} curve, with most of the data points lying closer to the α = 100 s^{-1} curve. This is in excellent agreement with the temperature vs. mixture fraction data in Figures 4 and 5.

The H_2 vs. O_2 data (averaged in mixture fraction intervals) are shown in Figure 7. The results at x/d = 10 and 25 deviate strongly from the AE curve while the data further downstream progressively approach the AE limit, (similar to the trends observed in Figure 5). The last point of comparison between the H_2 turbulent jet-diffusion flame data and the stretched laminar flamelet calculations of David et al.[9] is the value of OH concentrations shown in

Figure 8. Absolute OH concentrations were measured in the turbulent H_2 flame using single pulse laser-saturated OH fluorescence.[14] The maximum measured instantaneous OH concentration was 6.2 x 10^{16} molecules/cc. This value was found to be in reasonable agreement with the maximum value calculated for partial equilibrium conditions (5.5 x 10^{16} molecules/cc) and with the maximum of 6.4 x 10^{16} molecules/cc calculated by Warnatz[40] in a laminar premixed stoichiometric H_2-air flame. The measured value from the turbulent H_2 flame is compared to adiabatic equilibrium and stretched laminar flamelet calculations in Figure 8. At low values of stretch a = 100 s^{-1}, the maximum calculated OH concentration is 6.1 x 10^{16} molecules/cc, in excellent agreement with the measured maximum in turbulent flames. These values are far in excess of the adiabatic equilibrium value of 2.1 x 10^{16} molecules/cc, demonstrating the pronounced effect of free radical superequilibrium. Near extinction (a = 12,000 s^{-1}), the calculated OH concentration drops, but it is still considerably above the AE values.

3.4.4 $CO/H_2/N_2$ Flames

Some of the pulsed-Raman measurements of temperature vs. hydrogen element mixture fraction are shown in Figures 9 and 10. The pulsed-Raman measurements of temperature in the $CO/H_2/N_2$ flames contain an unresolved inconsistency. Temperatures measured by the sum of the mole fractions from Stokes vibrational Raman intensities (data shown in Figures 9 and 10) are as much as 15% lower than temperatures measured by the Stokes-antiStokes ratio method. Since the same effect occurs in laminar and turbulent flames, this discrepancy should not change the relative comparisons shown in Figures 9 and 10. Because the stoichiometric mixture fraction for this fuel mixture is 0.3 (as compared to 0.0283 for H_2), its turbulent flame length is much less ($x/d \leq 50$) than the H_2

flame length (x/d ~ 150). Results for x/d = 10, 25, and 50 and are compared in Figure 9 to an adiabatic equilibrium flame calculation for the fuel burning in air. The deviations from AE are much larger in the $CO/H_2/N_2$ flames than in the H_2 flame. For example, peak flame temperatures are 1600 K at x/d = 10 while the maximum AE temperature is 2240 K. Although no evidence of localized extinction is found, the measured temperatures in very fuel rich regions (ξ ~ 0.7) at x/d = 10, are not much above room temperature while the AE calculated temperature is ~ 1000 K. Averaging in mixture fraction intervals gives the values shown in Figure 10. Even far downstream at x/d = 50, the measured temperatures are 200-400 K lower than the AE calculations.

The dashed line in Figure 10 corresponds to experimental Raman measurements in our laboratory from a laminar opposed-flow diffusion flame. The fuel enters the combustor through a (5 cm long by 3 cm external radius) porous sintered copper cylinder. The molar fuel composition is $40\%CO/30\%H_2/30\%N_2$ and the cold flow fuel velocity is 8.77 cm/s. The inlet air velocity is 1.05 m/s corresponding to an approximate velocity gradient of $a = 2V/R = 70\ s^{-1}$. Measurement techniques applied to this and other laminar opposed-flow diffusion flames include coated fine-wire thermocouples, laser velocimetry, NO and NO_x probe sampling, gas chromatography, and pulsed-Raman scattering. Details are presented elsewhere.[18] Only a limited set of pulsed-Raman data are presented here in Figures 10-12 for comparison with the turbulent flame data. The laminar-flame data in Figure 10 show a peak flame temperature of only 1650 K. As was found in the H_2 flames, the turbulent flame data lie in a reasonably narrow band largely between the laminar-flame curve and the adiabatic equilibrium curve. The turbulent flame data also lie closer to the AE curve farther downstream in the flame.

Because individual molecular concentrations are measured by pulsed-Raman scattering, the conversion of H_2 into H_2O and of CO into CO_2 can be monitored separately. Conditionally averaged measurements of the fractional conversion of H_2 (defined as the mole fraction of H_2O divided by the sum of the H_2 and H_2O mole fractions) are shown in Figure 11 and the corresponding values for CO conversion shown in Figure 12. The conversion of H_2 measured in the turbulent flame is approximately the same as calculated from adiabatic equilibrium. The CO conversion (shown in Figure 12) shows much larger deviations from adiabatic equilibrium both in the laminar and turbulent flame data. As before, the turbulent flame data in general lie between the laminar-flame data and the AE curve.

3.4.5 Conclusions

It has been shown that finite-rate chemistry processes (three-body radical recombination and CO to CO_2 conversion) are important in turbulent jet-diffusion flames, even for H_2 and CO fuels and at the relatively low Reynolds number of 8500. Finite-rate chemistry processes are expected to be even more important for hydrocarbon fuels and for high Reynolds number flames.

In H_2 flames, the instantaneous correlations of temperature and mixture fraction in the turbulent Re = 8500 flame close to the fuel nozzle (i.e., at x/d = 10 or 25) show temperatures as much as 300 K less than those calculated at adiabatic equilibrium. The temperature-mixture fraction correlation approaches equilibrium far downstream (i.e., at x/d = 200). Instantaneous or conditionally averaged mole fractions of H_2 and O_2 show substantial coexistence of H_2 and O_2 close to the nozzle (at x/d = 10 and 25) but to a much more limited extent farther downstream. These trends are consistent with OH concentration measurements which are a factor of 3 larger than equilibrium

close to the nozzle but approach equilibrium far downstream.

These turbulent H_2 flame data are compared with stretched laminar flamelet calculations[9] including detailed chemical kinetic and transport processes for H_2 flames at two values of flame stretch (α = 100 and α = 12,000 s^{-1}). The α = 12,000 s^{-1} flame is calculated to be near the stretch-induced extinction limit. The stretched laminar flamelet calculations also show the same effects--reduced peak flame temperatures, substantial coexistence of H_2 and O_2, and large superequilibrium OH radical concentrations. In nearly all cases in Figures 4-7, the turbulent diffusion flame data lie intermediately between the (α = 12,000 s^{-1} laminar-flame calculation and the calculated adiabatic equilibrium curve. A few data points out of several thousand measurements fall above the α = 12,000 s^{-1} curves in Figure 6 (which David et al.[9] find to be the stretch-induced extinction limit). This may indicate a few isolated cases of localized extinction. However, the Raman data above the α = 12,000 s^{-1} curve may also arise from experimental errors due to background or measurement uncertainties (this is particularly true of data points in the upper left-hand corner of Figure 6 where the measured mole fraction of H_2 is less than 0.01) or to a nonhomogeneous sample in the Raman measurement volume.

Radical concentrations in turbulent flames appear also to be representable using the laminar flamelet approach. The peak OH concentration calculated for the α = 100 s^{-1} stretched laminar flames is 6.1 x 10^{16} molecules/cc in excellent agreement with the maximum OH concentration (6.2 x 10^{16} molecules/cc) measured by laser-saturated fluorescence in the turbulent flame. Both values are several times larger than the maximum OH concentration of 2.1 x 10^{16} molecules/cc calculated assuming adiabatic equilibrium. The α = 100 s^{-1} flame with a peak temperature of 2285 K has calculated radical

concentrations which are close to partial equilibrium (i.e., agree closely with Eqns. 1-3 in Ref. 14), while the radical concentrations in the α = 12,000 s^{-1} flame (with a peak temperature of 1400 K) are not in partial equilibrium. Direct measurements in turbulent diffusion flames of deviations from partial equilibrium are not available. However, the results shown in the laminar flame agree with calculations by Warnatz[40] in stoichiometric laminar premixed H_2-air flames where partial equilibrium prevailed when temperatures were greater than 1500 K, but showed marked deviations at lower temperatures. Similar deviations in partial equilibrium are to be expected in turbulent diffusion flames. The above comparisons confirm that very large superequilibrium radical concentrations occur in laminar and turbulent H_2 diffusion flames and that stretched laminar flamelet approaches should apply to the near nozzle regions of turbulent diffusion flames. Indeed, the stretched laminar flamelet approach may more accurately represent the primary reaction zones of turbulent flames than does the two-scalar pdf approach because the laminar flamelet approach does not need to assume partial equilibrium and can in principle account properly for localized extinction, if it occurs.

The decay of superequilibrium radicals back to equilibrium is known to occur by relatively slow three-body recombination reactions. Even in a mildly stretched (α = 100 s^{-1}) laminar-diffusion flame, the residence time in the reaction zone is not long enough for the three-body recombinations to equilibrate the radical concentrations. Thus, in turbulent flames it seems likely that these three-body recombination reactions will occur over wide regions of the flame and not just in localized laminar flamelets. This will complicate the application of the laminar flamelet approach in turbulent jet flames. The second factor that complicates the quantitative comparison of turbulent and

stretched laminar flamelet calculations in H_2 flames is the process of preferential diffusion. This process has a significant effect in laminar-diffusion flames[9] and was found to be important in low Reynolds number turbulent H_2-diffusion flames.[19] Its importance was found to decrease as Re increases, but because turbulent flames consist of a wide range of length and time scales, preferential diffusion may always occur to some extent in turbulent flames with H_2 fuel. Comparison of laminar-flame calculations and turbulent flame data in Figure 5 confirm that preferential diffusion accounts for some of the differences between laminar- and turbulent-H_2 flames.

In the 40%CO/30%H_2/30%N_2 flames, the instantaneous correlations of temperature and mixture fraction in the turbulent Re = 8500 flame show temperatures as much as 650 K less than calculated at adiabatic equilibrium close to the fuel nozzle. The temperature-mixture fraction correlation is still far from equilibrium downstream of the turbulent flame at x/d = 50. Instantaneous or conditionally averaged measurements of $X(H_2O)/(X(H_2) + X(H_2O))$ and $X(CO_2)/(X(CO) + X(CO_2))$ show that the conversion of H_2 is much closer to equilibrium than the conversion of CO and that the conversion of CO remains far from equilibrium at x/d = 50. Although not shown in this report, mean OH concentration measurements in this flame, published previously,[6] are six times larger than equilibrium near the fuel nozzle (x/d = 10) and remain four times larger than equilibrium at x/d = 50.[6]

Comparisons of the laminar and turbulent $CO/H_2/N_2$ flames suggest the same trends as described for the H_2 flames-- namely that the turbulent flame data lie between the stretched laminar flame relationship and the adiabatic equilibrium curve and move toward the AE curve far downstream. The laminar flamelet approach to turbulent combustion modeling is expected to be better in reaction

zones than the two-scalar model because it does not need to make partial equilibrium assumptions. However, chemical reactions which are much slower (i.e., three-body recombinations for the decay of superequilibrium or for HO_2 formation as well as CO burn-out in relatively cool gas) might be difficult to incorporate into laminar flamelet models. For example, the two-scalar pdf model (which assumed that CO was in partial equilibrium with the radical pool) calculated mean temperatures and OH concentrations in much better agreement with experiment than a one-scalar equilibrium model, confirming the increased importance of superequilibrium when substantial CO is present in the fuel. However, the two-scalar model overpredicts mean temperature and OH concentration values in predominantly low-temperature fuel-rich regions and predicts the approach to equilibrium is faster than measured. These discrepancies may be due to the assumption that CO is in partial equilibrium with the radical pool. Warnatz[39] has demonstrated that in premixed laminar-flame calculations, deviations from partial equilibrium are much larger in CO-containing flames, and that deviations occur at much larger temperatures (i.e., 1800 K for CO instead of 1500 K for H_2 flames). The two-scalar model also predicts higher mean temperatures and higher OH concentrations in predominantly cool zones, perhaps due to the neglect of HO_2 formation. It is not clear whether the laminar flamelet approach will be an improvement over two-scalar models for HO_2 predictions.

Finally, it should be mentioned that the pulsed-Raman data or planar-induced OH fluorescence imaging measurements have shown that localized extinction is not an important phenomena in the simple H_2 or $CO/H_2/N_2$ turbulent jet-diffusion flames discussed here. This is in sharp contrast to the extensive localized extinction found in pilot-flame stabilized hydrocarbon turbulent

jet-diffusion flames using planar-fluorescence imaging[10] and pulsed-Raman scattering.[11] These results are not contradictory. Fuels containing large amounts of H_2 have high H-atom concentrations in their reaction zones and must be very highly stretched (i.e., $a \cong 12{,}000\ s^{-1}$ for H_2) before extinction occurs (i.e., when $H + O_2 \rightarrow HO + O$ becomes too slow to generate sufficient radical concentrations). Hydrocarbon fuels are extinguished at much lower values of stretch ($a \cong 375\ s^{-1}$ for CH_4) so localized extinction is expected to be more prevalent in turbulent hydrocarbon flames. However, the most important difference between the two sets of experiments is the pilot-flame stabilization. In a simple jet (with no pilot-flame stabilization) extinction is most likely to occur at the nozzle exit where the shear rates are highest; the amount of extinction should decrease downstream. Increasing the shear rate by increasing the fuel velocity causes the flame to blow off. The pilot-flame stabilization permits attached flames at high stretch rates so localized extinction can occur downstream of the nozzle. The stretched laminar flamelet approach to turbulent combustion modeling should work well even under conditions of localized extinction--provided experiment or model calculations of the laminar-diffusion flame structures are available near the extinction limit. However, published versions of laminar flamelet models do not account specifically for the partial fuel-air mixing and subsequent burning which occur due to localized extinction.

The laminar opposed-flow diffusion flame experiments were sponsored by the Basic Research Department of the Gas Research Institute under Contract 5081-263-0600 (Mr. James Kezerle, Program Manager).

3.5 High Reynolds Number Flame Facility

The objective here is to develop and qualify a turbulent jet diffusion flame burner which will support combustion at Reynolds numbers high enough for significant local stretch-induced extinction to be expected. Localized extinction is unimportant in coflowing H_2 jet/air flames as only a few instantaneous Raman measurements of temperature or of H_2-O_2 overlap are close to that calculated at extinction (α = 12000 s^{-1}). This agrees with previous OH planar laser induced fluorescence measurements which showed <u>continuous</u> flame fronts.

For extensive localized extinction to be present stabilized flames or lifted flames can be used. Previous measurements on H_2 or $CO/H_2/N_2$ jet diffusion flames used a simple pipe (id= 3.18 mm) with its exterior machined to a fine edge. Above Re ~ 9000, blow-off occurred. A double concentric fuel nozzle has therefore been built with a 3.18 mm id inner pipe and 5.5 mm id external pipe. The presence alone of the outer pipe permitted stabilization of H_2 flames in the inner pipe to Re=17,000 and resulted in lifted flames. The addition of an H_2 <u>diffusion</u> flame pilot with a fuel velocity of 1% of the main flow velocity stabilized H_2 flames at Re=20,000. Extensive localized extinction effects may be present in these flames.

Because H_2 fuel is characterized by high burning velocities and, therefore, high stretch before extinction would occur, experiments are being performed to reduce the amount of H_2 in the $CO/H_2/N_2$ mixtures. This will maximize the probability of finding stretch-induced extinction in the turbulent jet flame.

3.3 High Reynolds Number Flame Facility

The objective here is to develop and qualify a turbulent jet diffusion flame burner which will support combustion at Reynolds numbers high enough for significant local stretch-induced extinction to be expected. Localized extinction is unimportant in coflowing H_2 jet/air flames as only a few instantaneous Raman measurements of temperature or of H_2-O_2 overlap are close to that calculated at extinction (α = 12000 s^{-1}). This agrees with previous OH planar laser induced fluorescence measurements which showed <u>continuous</u> flame fronts.

For extensive localized extinction to be present stabilized flames or lifted flames can be used. Previous measurements on H_2 or $CO/H_2/N_2$ jet diffusion flames used a simple pipe (id= 3.18 mm) with its exterior machined to a fine edge. Above Re ~ 9000, blow-off occurred. A double concentric fuel nozzle has therefore been built with a 3.18 mm id inner pipe and 5.5 mm id external pipe. The presence alone of the outer pipe permitted stabilization of H_2 flames in the inner pipe to Re=17,000 and resulted in lifted flames. The addition of an H_2 <u>diffusion</u> flame pilot with a fuel velocity of 1% of the main flow velocity stabilized H_2 flames at Re=20,000. Extensive localized extinction effects may be present in these flames.

Because H_2 fuel is characterized by high burning velocities and, therefore, high stretch before extinction would occur, experiments are being performed to reduce the amount of H_2 in the $CO/H_2/N_2$ mixtures. This will maximize the probability of finding stretch-induced extinction in the turbulent jet flame.

3.6 Related Work

The present turbulent $CO/H_2/N_2$ jet diffusion flame data has been used to compare with thermal nitric oxide predictions at high Reynolds number (Reference C in Section 4), with a turbulent combustion model using Monte Carlo methods with the two-scalar partial-equilibrium model (Pope and Correa, Reference D in Section 4) and using a new three-scalar assumed shape pdf model (Correa).[7] The Monte Carlo results (Pope and Correa) demonstrated strong correlation between the two-scalar variables (ξ and η) and were in somewhat better agreement with the experimental data than the previous two-scalar assumed-shape pdf approach which assumed the two variables were uncorrelated. The three scalar assumed shape pdf calculations (Correa)[7] separated the reaction $CO + OH \longrightarrow CO_2 + H$ from the partially equilibrated radical pool and gave calculated results in somewhat better agreement with experiment than the previous two-scalar pdf approach.

4. Publications and Presentations Supported by AFOSR Contract

A. Drake, M. C., "Stretched Laminar Flamelet Analysis of Turbulent H_2 and $CO/H_2/N_2$ Diffusion Flames," accepted for Twenty-first Symp. (Int.) on Combustion, 1986.

B. Drake, M. C. and Fenimore, C. P., "Stretched Laminar Opposed-Flow Diffusion Flame Experiments: Extinction and Nitric Oxide Formation," to be submitted for publication, 1986.

Related Publications and Presentations

C. Correa, S. M., "Nitric Oxide Formation and Turbulent Flame Structure,"

presented at 1985 Eastern States Section/Combustion Institute.

D. Pope, S. B. and Correa, S. M., "Joint Pdf Calculations of a Non-Equilibrium Turbulent Diffusion Flame," accepted for Twenty-first Symp. (Int.) on Combustion, 1986.

5. Professional Personnel

The following personnel contributed to this research:

(i) Dr. M. C. Drake (until May 23, 1986)

(ii) Dr. S. M. Correa

(iii) Mr. Frank Haller

References

1. R.W. Bilger, Prog. Energy Combust. Sci. 1, 87, 1976.

2. R.W. Bilger, Combust. Flame 30, 277, 1977.

3. R.W. Bilger and S.H. Starner, Combust. Flame 51, 155, 1983.

4. S.D. Burke and T.E.W. Schumann, Ind. Eng. Chem. 20, 998, 1928.

5. G.F. Carrier, F.E. Fendell, and F.E. Marble, "The Effect of Strain on Diffusion Flames," Project SQUID Technical Report TRW-5-PN, SIAM J. App. Math., Oct. 1973.

6. S.M. Correa, M.C. Drake, R.W. Pitz, and W. Shyy, Twentieth Int. Combust. Symp., The Combustion Institute, 337, 1984.

7. S.M. Correa, "A Model for Nonpremixed Turbulent Combustion of CO/H_2 Jets," Ninth International Symposium on Combustion Processes, Wisla-Jawornik, Poland, to appear in Archivuum Combustionis.

8. G. Damköhler, J. Electrochem. 46, 601, 1940.

9. T. David, P.H. Gaskell, and G. Dixon-Lewis, "Structure and Properties of Methane-Air and Hydrogen-Air Counterflow Diffusion Flames," submitted for publication.

10. R.W. Dibble, M.B. Long, A. Masri, Two Dimensional Imaging of C_2 in Turbulent Nonpremixed Flames, Tenth Int. Colloquium on Dynamics of Explosions and Reactive Systems, Berkeley, CA, August 1985.

11. R.W. Dibble, A. Masri, and R.W. Bilger, "Spontaneous Raman Measurements in Laminar and Turbulent Nonpremixed Flames of Methane," submitted for publication. See also Figure 16 of Reference 5.

12. G. Dixon-Lewis, T. David, P.H. Gaskell, S. Fukutani, H. Jinno, J.A. Miller, R.J. Kee, M.D. Smooke, N. Peters, E. Effelsburg, J. Warantz, and F. Behrendt, Twentieth Int. Combust. Symp., The Combustion Institute, 1893, 1984.

13. M.C. Drake, R.W. Bilger, and S.H. Starner, Nineteenth Int. Combust. Symp., The Combustion Institute, Pittsburgh, 459, 1982.

14. M.C. Drake, R.W. Pitz, M. Lapp, C.P. Fenimore, R.P. Lucht, D.W. Sweeney, and N.M. Laurendeau, Twentieth Int. Combust. Symp., The Combustion Institute, 327, 1984.

15. M.C. Drake and W. Kollmann, "Slow Chemistry Nonpremixed Flows," Evaluation of Data on Simple Turbulent Reacting Flows (W.C. Strahle, ed.), AFOSR TR-85 0880, Sept. 1985.

16. M.C. Drake and R.W. Pitz, Experiments in Fluids 3, 283, 1985.

17. M.C. Drake, R.W. Pitz, and W. Shyy, "Conserved Scalar PDFs in a Turbulent Jet Diffusion Flame," Turbulent Shear Flows V, 10.13, 1985; accepted for publication in J. Fluid Mechanics.

18. M.C. Drake, Kinetics of Nitric Oxide Formation in Laminar and Turbulent Methane Combustion, Gas Research Institute Final Report, 1985.

19. M.C. Drake, R.W. Pitz, and M. Lapp, "Laser Measurements on Nonpremixed Hydrogen-Air Flames for Assessment of Turbulent Combustion Models," AIAA Paper 84-0544, accepted for publication AIAA J.

20. H.E. Eickhoff and K. Grethe, Combust. Flame 35, 267, 1977.

21. G.M. Faeth and G.S. Samuelsen, "Fast Reaction Nonpremixed Combustion," Evaluation of Data on Simple Turbulent Reacting Flows (W.C. Strahle, ed.) AFOSR TR-85 0880, Sept. 1985.

22. J. Janicka and W. Kollmann, Combust. Flame 44, 319, 1982.

23. S-M. Jeng, L-D. Chen, and G.M. Faeth, Nineteenth Int. Combust. Symp., The Combustion Institute, 349, 1982.

24. W.P. Jones and J.H. Whitelaw, Combust. Flame 48, 1, 1982.

25. G. Kychakoff, R.D. Howe, R.K. Hanson, M.C. Drake, R.W. Pitz, M. Lapp, and C.M. Penney, Science 224, 382, 1984.

26. P.A. Libby and F.A. Williams, ed., Turbulent Reacting Flows, Springer-Verlag, New York, 1980.

27. S.K. Liew, K.M.C. Bray, and J.B. Moss, Combust. Sci. Tech. 27, 69, 1981.

28. S.K. Liew, K.M.C. Bray, and J.B. Moss, Combust. Flame 56, 199, 1984.

29. A. Linan, Acta Astronautica 1, 1007, 1974.

30. F.E. Marble and J.E. Broadwell, A Theoretical Analysis of Nitric Oxide Production in a Methane/Air Turbulent Diffusion Flame, EPA-600/7-80-018.

31. J.A. Miller, R.J. Kee, M.D. Smooke, and J.F. Grear, "The Computation of the Structure and Extinction Limit of a Methane-Air Stagnation Point Diffusion Flame," Western States/CI Paper 84-20, 1984.

32. R.E. Mitchell, A.F. Sarofim, and L.A. Clomburg, Combust. Flame 37, 227, 1980.

33. R.E. Mitchell, A.F. Sarofim, and L.A. Clomburg, Combust. Flame 37, 201, 1980.

34. R.E. Mitchell, A.F. Sarofim, and R. Yu, Combust. Sci. Tech. 21, 157, 1980.

35. N. Peters, ''Laminar-Diffusion Flamelet Models in Non-premixed Turbulent Combustion,'' Progress in Energy and Combustion Science 10, 319, 1984.

36. R.W. Pitz and M.C. Drake, ''Intermittency and Conditional Averaging in a Turbulent Nonpremixed Flame by Raman Scattering,'' AIAA Paper 84-0197, accepted for publication AIAA J.

37. M.K. Kazdan and J.G. Stevens, Combust. Flame 59, 289, 1985.

38. H.T. Tsuji and I. Yamaoki, Thirteenth Int. Combust. Symp., The Combustion Institute, 189, 1971.

39. J. Warnatz, Ber. Bunsenges. Phys. Chem. 83, 950, 1979.

40. J. Warnatz, Combust. Sci. Tech. 26, 203, 1981.

41. F.A. Williams, ''Recent Advances in Theoretical Descriptions of Turbulent Diffusion Flames,'' Turbulent Mixing in Nonreactive and Reactive Flows (S.N.P. Murthy, ed.), Plenum Press, 189, 1974.

Figure Captions

Figure 1 Comparison of temperatures measured by radiation-corrected thermocouples and by pulsed Raman scattering.

Figure 2 Apparent CO_2 mole fraction from measured CO_2 Stokes vibrational Raman intensity.

Figure 3 Comparison of previous with reanalyzed Raman data.

Figure 4 Instantaneous measurements of temperature and mixture fraction using pulsed-laser-Raman scattering from the H_2 turbulent jet-diffusion flame. Each of the ~30,000 points represents one time (2μs) and space ($<0.1\ mm^3$) resolved measurement. Data from three axial positions (x/d = 10, 50 and 200) are shown. The solid line is the calculated relationship between temperature and mixture fraction in H_2-air flames under adiabatic equilibrium conditions.

Figure 5 Data conditionally-averaged in mixture fraction intervals from the H_2 turbulent jet-diffusion flame at all six axial locations measured. The solid line is the same as in Figure 4. The dotted lines are those calculated by David et al.[9] for laminar opposed-flow H_2 diffusion flames under small stretch ($a = 100\ s^{-1}$) and near extinction ($a = 12{,}000\ s^{-1}$).

Figure 6 Instantaneous measurements of O_2 and H_2 mole fractions using pulsed-laser-Raman scattering from the H_2 turbulent jet-diffusion flame close to the fuel exit at x/d = 10 and 25. The solid and dashed curves are the same as in Figure 5.

Figure 7 Data conditionally-averaged in mixture fraction intervals in the H_2 turbulent jet-diffusion flame showing the copresence of H_2 and O_2.

Figure 8 The OH concentrations versus mixture fraction calculated assuming adiabatic equilibrium (solid curve) and calculated by David et al.[9] for laminar-opposed flow H_2 diffusion flames under small stretch ($a = 100\ s^{-1}$) and near extinction ($a = 12{,}000\ s^{-1}$). The maximum instantaneous OH concentration measured by laser-saturated fluorescence in the Re = 8500 H_2 turbulent jet-diffusion flame is shown by the solid horizontal line.

Figure 9 Instantaneous pulsed-Raman measurements of temperature and mixture fraction from a turbulent jet-diffusion flame with 40%CO/30%H_2/30%N_2 fuel. Temperatures were measured assuming the ideal gas law from the sum of the mole fractions of all major species measured by their respective Stokes vibrational Raman intensities. The solid line is the calculated adiabatic equilibrium curve for the CO/H_2/N_2 fuel mixture.

Figure 10 Conditionally-averaged Raman measurements of temperature and mixture fraction in the turbulent CO/H_2/N_2 jet diffusion flame at x/d = 10, 25 and 50 (data points) and from the laminar opposed-flow diffusion flame with the same fuel (dotted line).

Figure 11 Conditionally-averaged Raman measurements of the conversion of H_2 versus mixture fraction in the turbulent jet-diffusion flame and laminar opposed-flow diffusion flame with $CO/H_2/N_2$ fuel. Symbols are the same as in Figure 10.

Figure 12 Conditionally-averaged Raman measurements of the conversion of CO versus mixture fraction in the turbulent jet diffusion flame and laminar opposed-flow diffusion flame with $CO/H_2/N_2$ fuel. Symbols are the same as in Figure 10.

List of Tables

Table I Reanalyzed Raman data at x/d = 10 in $CO/H_2/N_2$.

**FILENAME=AMB10 3:55 PM MON., 1 JULY, 1985
**PROGRAM = RADF
**
**DATA REDUCED WITH PROGRAM &RLTC ON 07/01/85
**

**POS. (mm)	TEMP. (k)	CONCENTRATION - MOLES/CM3 (*E-7) CO2	O2	CO	N2	CH4	H2O	H2	DENSITY	FILE NAME
6.00	343.8	.53	77.68	-1.35	285.88	0.00	3.40	-.30	.9196	ACE2G
5.00	909.8	3.59	29.58	.74	126.22	0.00	8.63	-.13	.4198	ACE2H
4.00	1644.0	6.90	6.02	4.37	55.26	0.00	10.13	.64	.2044	ACE2F
3.00	1729.5	7.54	.45	15.19	46.02	0.00	10.77	4.99	.1963	ACE2I
2.00	1188.5	6.64	-.09	38.57	57.25	0.00	10.78	19.43	.2773	ACE2E
1.00	712.8	5.63	-.39	69.99	76.47	0.00	8.33	41.89	.3950	ACE2J
0.00	515.5	4.75	-.14	96.18	94.48	0.00	6.23	61.52	.4993	ACE2D
0.00	535.5	4.37	-.46	90.02	90.65	0.00	6.05	57.77	.4719	ACE2M
-1.00	629.9	4.89	-.47	80.65	83.02	0.00	7.27	49.05	.4331	ACE2K
-5.00	1073.3	4.35	21.73	.98	99.98	0.00	9.17	-.06	.3381	ACE2L

**FILENAME=BMB10 3:55 PM MON., 1 JULY, 1985
**PROGRAM = RADF
**
**DATA REDUCED WITH PROGRAM &RLTC ON 07/01/85
**

**POS. (mm)	TEMP. (k)	MOLE FRACTION CO2	O2	CO	N2	CH4	H2O	H2	MIXTURE FRAC. CONV.	FAVRE	FILE NAME
6.00	343.8	.002	.209	-.003	.773	0.000	.011	-.001	.006	.003	ACE2G
5.00	909.8	.032	.159	.007	.730	0.000	.063	-.001	.118	.087	ACE2H
4.00	1644.0	.085	.067	.052	.657	0.000	.123	.008	.290	.283	ACE2F
3.00	1729.5	.092	.007	.164	.550	0.000	.130	.051	.443	.450	ACE2I
2.00	1188.5	.056	-.001	.272	.444	0.000	.091	.133	.608	.622	ACE2E
1.00	712.8	.032	-.002	.335	.384	0.000	.048	.198	.716	.725	ACE2J
0.00	515.5	.021	-.001	.358	.362	0.000	.028	.227	.774	.779	ACE2D
0.00	535.5	.020	-.002	.356	.367	0.000	.028	.227	.761	.766	ACE2M
-1.00	629.9	.026	-.002	.349	.375	0.000	.039	.210	.733	.740	ACE2K
-5.00	1073.3	.042	.144	.010	.719	0.000	.078	0.000	.152	.125	ACE2L

Table II **Reanalyzed Raman data at x/d = 25 in $CO/H_2/N_2$.**

**FILENAME=AMB25 9:20 AM TUE., 2 JULY, 1985
**PROGRAM = RADF
**
**DATA REDUCED WITH PROGRAM &RLTC ON 07/02/85
**

**POS. (mm)	TEMP. (k)	CONCENTRATION - MOLES/CM3 (*E-7) CO2	O2	CO	N2	CH4	H2O	H2	DENSITY	FILE NAME
2.00	1463.5	8.18	.36	25.04	50.22	0.00	10.58	8.26	.2325	ACD2B
4.00	1599.6	8.49	.57	17.87	47.33	0.00	10.11	4.79	.2088	ACD2C
6.00	1647.7	8.91	3.06	11.01	51.11	0.00	9.20	2.10	.2082	ACD2D
8.00	1435.1	8.93	10.80	4.35	69.67	0.00	8.33	.34	.2576	ACD2E
10.00	1033.5	6.84	25.71	2.12	114.19	0.00	7.41	-.04	.3933	ACD2F
12.00	715.4	4.96	45.00	1.11	176.31	0.00	5.76	-.05	.5869	ACD2G
14.00	471.1	3.16	64.36	.08	243.35	0.00	3.92	-.15	.7927	ACD2H
16.00	322.0	1.52	84.14	-.57	310.03	0.00	2.07	-.11	1.0003	ACD2I
18.00	294.2	1.36	88.36	-.81	326.04	0.00	1.72	-.14	1.0495	ACD2J
0.00	1412.2	8.16	-.09	24.47	48.28	0.00	10.99	8.40	.2258	ACD2K
-4.00	1580.1	9.72	3.70	9.17	53.18	0.00	9.30	1.58	.2138	ACD2L

**FILENAME=BMB25 9:20 AM TUE., 2 JULY, 1985
**PROGRAM = RADF
**
**DATA REDUCED WITH PROGRAM &RLTC ON 07/02/85
**

**POS. (mm)	TEMP. (k)	MOLE FRACTION CO2	O2	CO	N2	CH4	H2O	H2	MIXTURE FRAC. CONV.	FAVRE	FILE NAME
2.00	1463.5	.082	.004	.234	.493	0.000	.105	.076	.443	.448	ACD2B
4.00	1599.6	.097	.007	.190	.536	0.000	.114	.049	.380	.386	ACD2C
6.00	1647.7	.108	.032	.125	.596	0.000	.109	.023	.285	.279	ACD2D
8.00	1435.1	.099	.087	.049	.663	0.000	.089	.004	.173	.151	ACD2E
10.00	1033.5	.061	.140	.020	.709	0.000	.062	0.000	.102	.074	ACD2F
12.00	715.4	.035	.176	.009	.735	0.000	.037	0.000	.057	.033	ACD2G
14.00	471.1	.017	.195	.002	.759	0.000	.019	-.001	.022	.011	ACD2H
16.00	322.0	.005	.208	-.001	.772	0.000	.007	0.000	.004	.002	ACD2I
18.00	294.2	.003	.210	-.002	.775	0.000	.004	0.000	.001	0.000	ACD2J
0.00	1412.2	.083	-.001	.235	.487	0.000	.112	.079	.469	.473	ACD2K
-4.00	1580.1	.116	.035	.106	.608	0.000	.110	.018	.264	.254	ACD2L

Table III Reanalyzed Raman data at x/d = 50 in $CO/H_2/N_2$.

**FILENAME=AMB50:FH:CD 11:57 AM TUE., 2 JULY, 1985
**PROGRAM = RADF
**
**DATA REDUCED WITH PROGRAM &RLTC ON 07/02/85
**

**POS. (mm)	TEMP. (k)	CONCENTRATION - MOLES/CM3 (*E-7) CO2	O2	CO	N2	CH4	H2O	H2	DENSITY	FILE NAME
2.00	1685.0	10.54	6.35	1.83	55.76	0.00	7.80	-.06	.2104	BCF2DD
4.00	1648.6	10.28	7.52	1.58	58.78	0.00	7.85	-.05	.2195	BCF2EE
6.00	1548.4	9.89	8.89	1.40	63.23	0.00	8.00	-.12	.2325	BCF2FF
8.00	1463.3	9.12	10.73	1.16	67.49	0.00	7.55	-.15	.2439	BCF2GG
10.00	1359.2	8.45	13.36	.99	75.20	0.00	7.68	-.12	.2673	BCF2HH
12.00	1202.4	8.10	16.96	.83	87.96	0.00	7.96	-.24	.3073	BCF2II
14.00	1020.9	6.89	23.37	.64	109.15	0.00	7.66	-.18	.3715	BCF2JJ
16.00	852.8	6.06	30.48	.28	132.56	0.00	7.45	-.17	.4443	BCF2KK
18.00	746.9	5.53	35.22	.25	148.47	0.00	7.23	-.10	.4940	BCF2LL
20.00	700.8	5.23	39.65	.11	163.25	0.00	6.92	-.14	.5405	BCF2MM
22.00	577.8	4.02	49.53	-.23	198.44	0.00	6.13	-.17	.6475	BCF2NN
24.00	491.2	3.21	59.25	-.76	229.95	0.00	5.48	-.11	.7463	BCF2PP
26.00	407.2	2.22	68.85	-1.25	265.08	0.00	4.74	.20	.8531	BCF2QQ
28.00	335.7	1.52	80.04	-1.56	302.43	0.00	3.94	-.13	.9709	BCF2RR
0.00	1764.1	10.23	5.42	1.20	54.65	0.00	7.58	-.13	.2021	BCF2SS
-4.00	1643.9	10.50	6.42	.50	58.17	0.00	7.59	-.10	.2129	BCF2TT
2.00	1792.0	7.22	5.89	2.73	52.63	0.00	7.08	.41	.1901	BCF2UU

**FILENAME=BMB50:FH:CD 11:57 AM TUE., 2 JULY, 1985
**PROGRAM = RADF
**
**DATA REDUCED WITH PROGRAM &RLTC ON 07/02/85
**

**POS. (mm)	TEMP. (k)	MOLE FRACTION CO2	O2	CO	N2	CH4	H2O	H2	MIXTURE FRAC. CONV.	FAVRE	FILE NAME
2.00	1685.0	.134	.070	.024	.669	0.000	.097	-.001	.188	.182	BCF2DD
4.00	1648.6	.126	.079	.020	.674	0.000	.093	0.000	.180	.174	BCF2EE
6.00	1548.4	.117	.086	.017	.681	0.000	.091	-.001	.172	.164	BCF2FF
8.00	1463.3	.107	.097	.014	.691	0.000	.084	-.001	.157	.144	BCF2GG
10.00	1359.2	.093	.112	.011	.698	0.000	.079	-.001	.151	.134	BCF2HH
12.00	1202.4	.080	.125	.009	.708	0.000	.073	-.002	.132	.114	BCF2II
14.00	1020.9	.060	.143	.006	.723	0.000	.061	-.002	.106	.085	BCF2JJ
16.00	852.8	.047	.158	.004	.733	0.000	.051	-.001	.084	.063	BCF2KK
18.00	746.9	.038	.167	.003	.740	0.000	.044	-.001	.069	.051	BCF2LL
20.00	700.8	.035	.172	.002	.743	0.000	.041	-.001	.062	.042	BCF2MM
22.00	577.8	.024	.182	.001	.754	0.000	.031	-.001	.040	.025	BCF2NN
24.00	491.2	.017	.190	-.001	.761	0.000	.025	0.000	.029	.016	BCF2PP
26.00	407.2	.010	.196	-.003	.769	0.000	.018	0.000	.017	.011	BCF2QQ
28.00	335.7	.006	.203	-.004	.774	0.000	.012	0.000	.006	.003	BCF2RR
0.00	1764.1	.134	.061	.016	.684	0.000	.098	-.002	.189	.184	BCF2SS
-4.00	1643.9	.133	.068	.006	.692	0.000	.094	-.001	.180	.173	BCF2TT
2.00	1792.0	.098	.069	.037	.687	0.000	.096	.005	.202	.194	BCF2UU

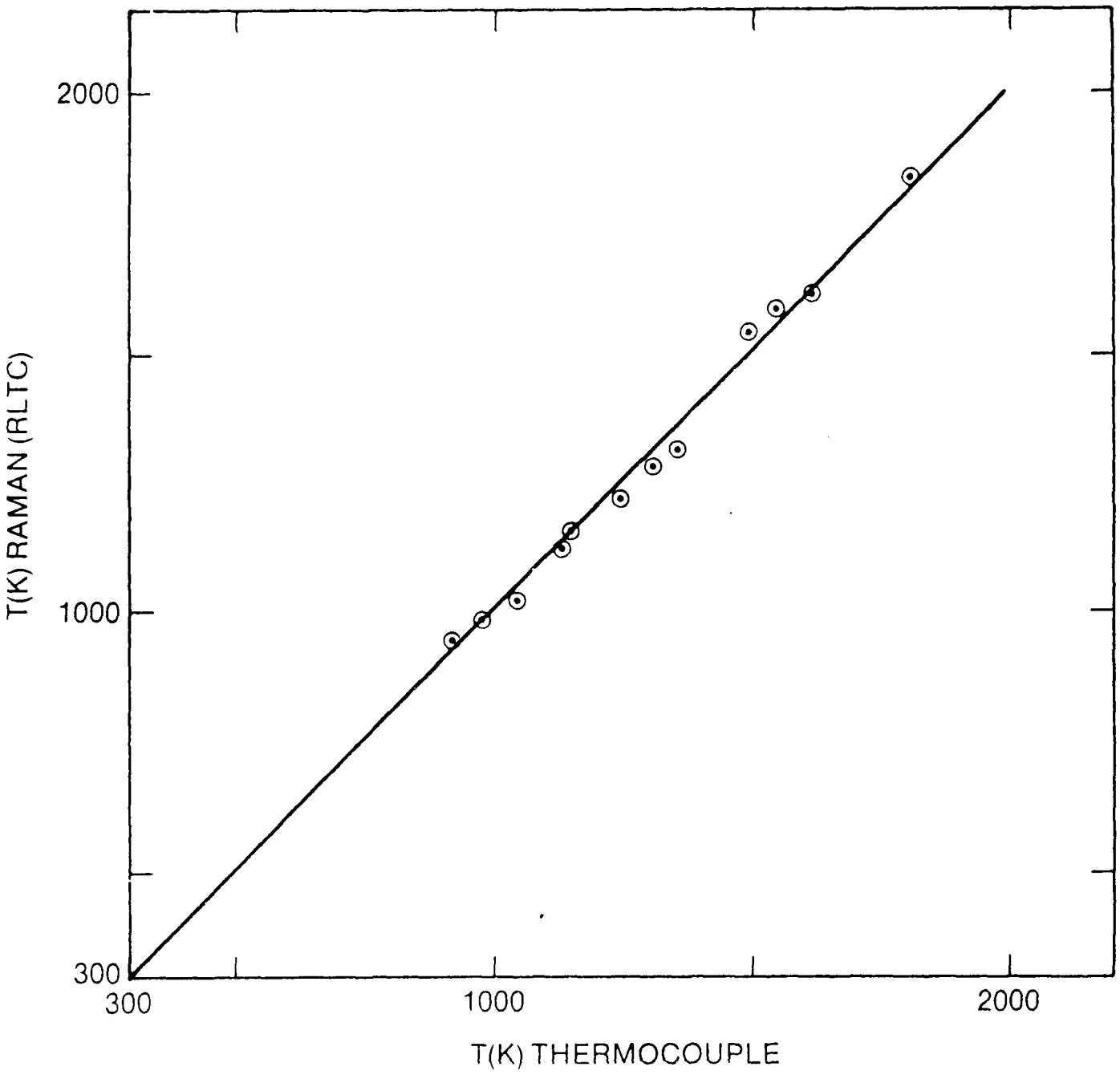

Figure 1 Comparison of temperatures measured by radiation-corrected thermocouples and by pulsed Raman scattering.

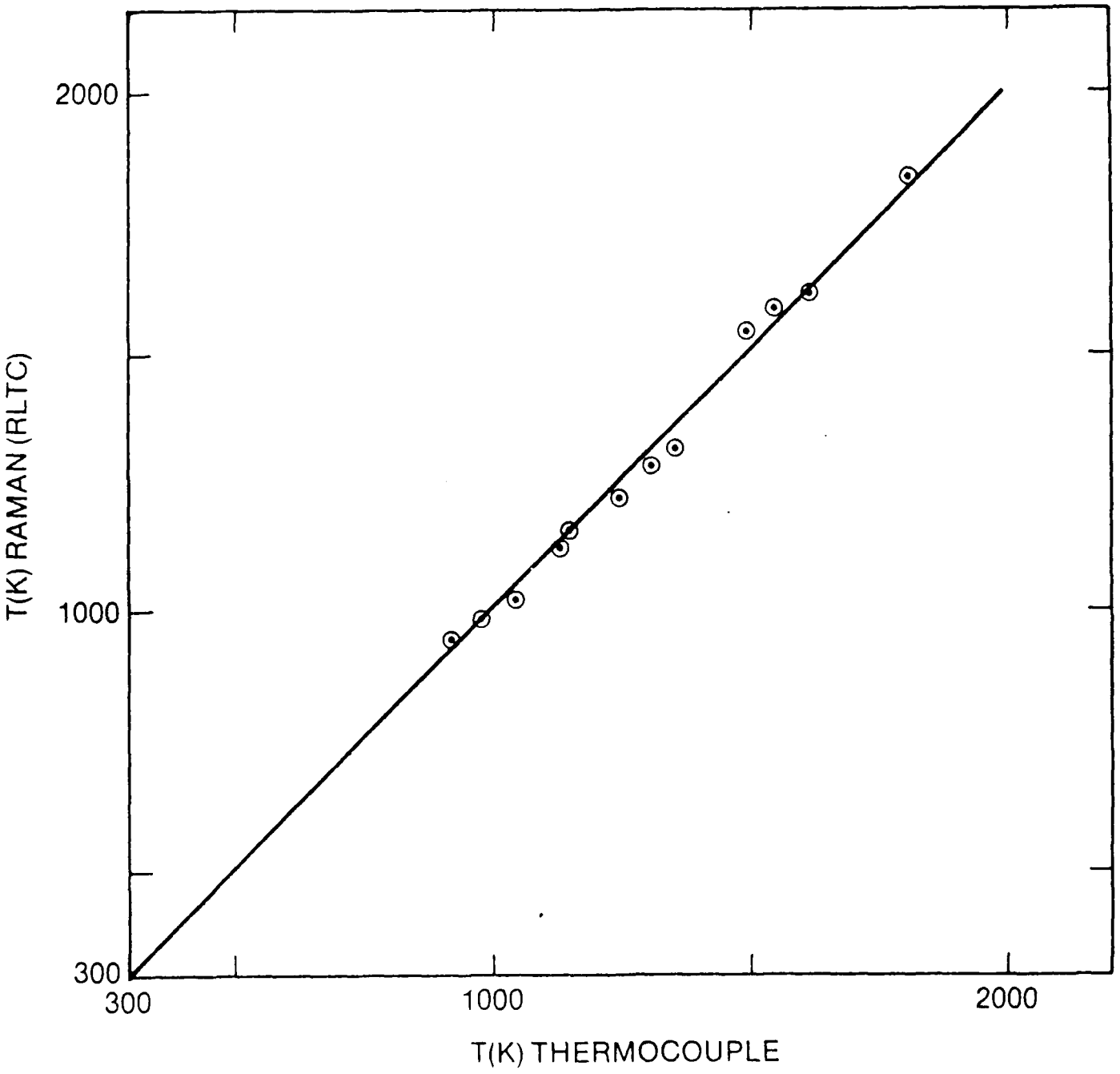

Figure 1 Comparison of temperatures measured by radiation-corrected thermocouples and by pulsed Raman scattering.

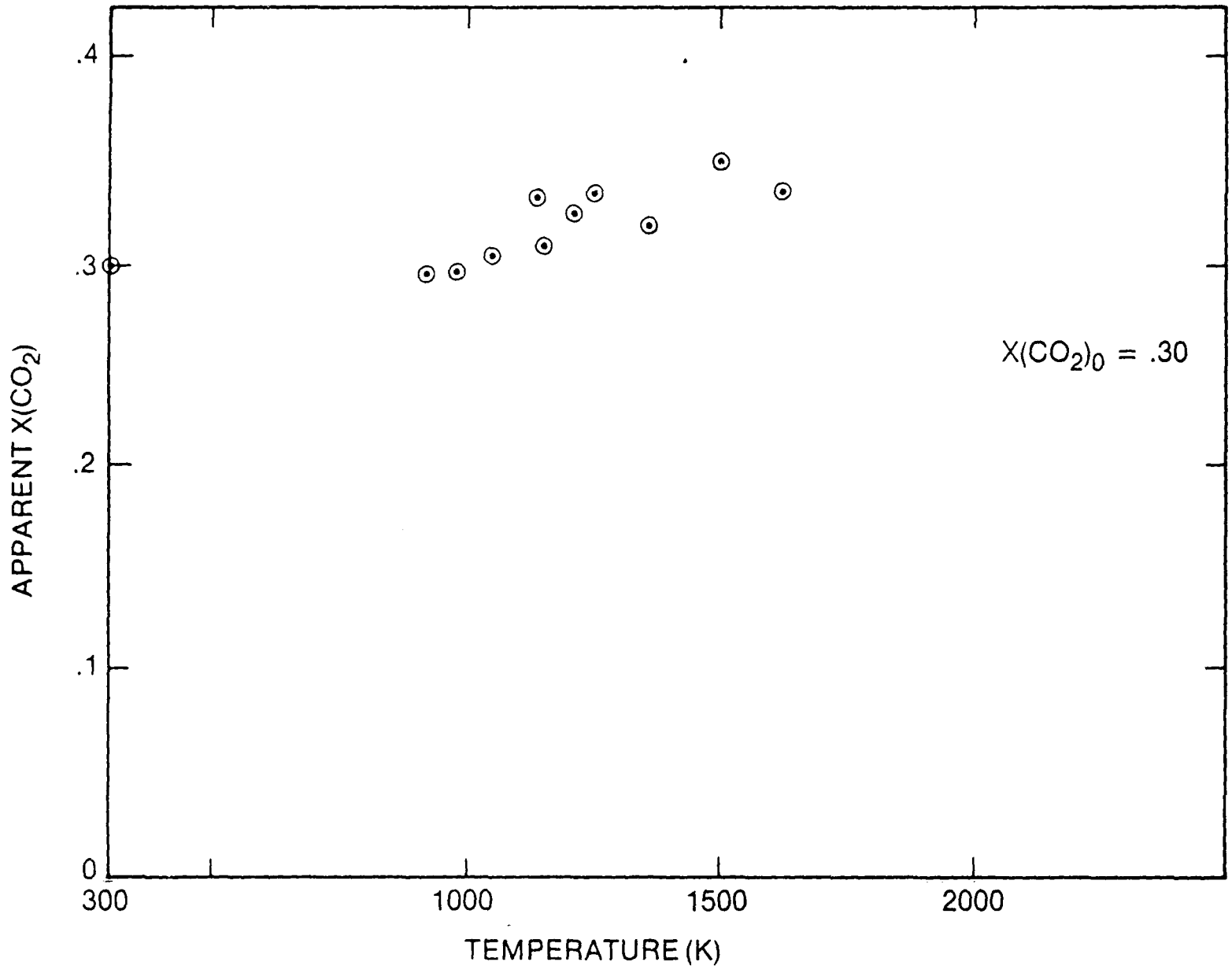

Figure 2 Apparent CO_2 mole fraction from measured CO_2 Stokes vibrational Raman intensity.

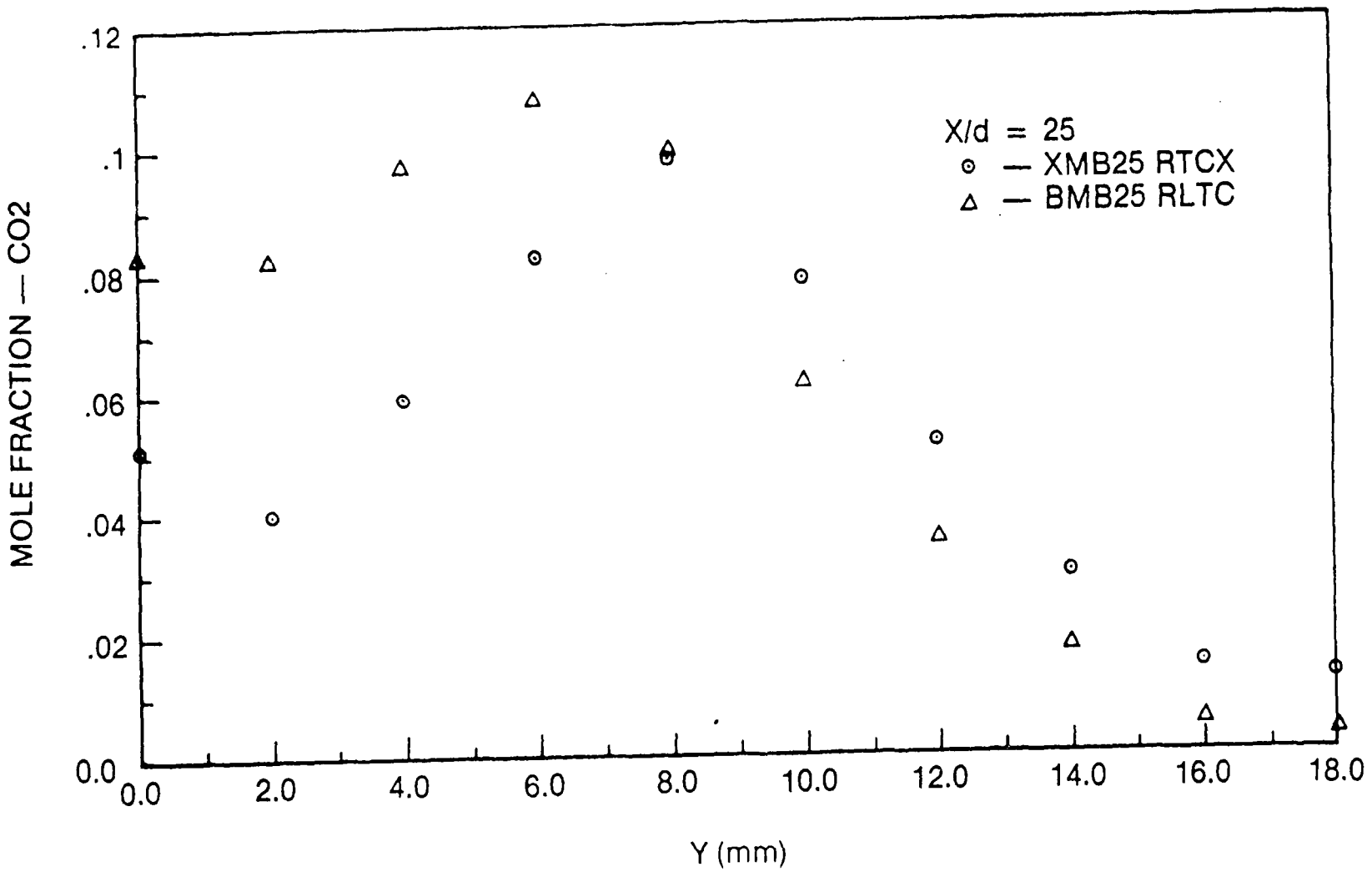

Figure 3 Comparison of previous with reanalyzed Raman data.

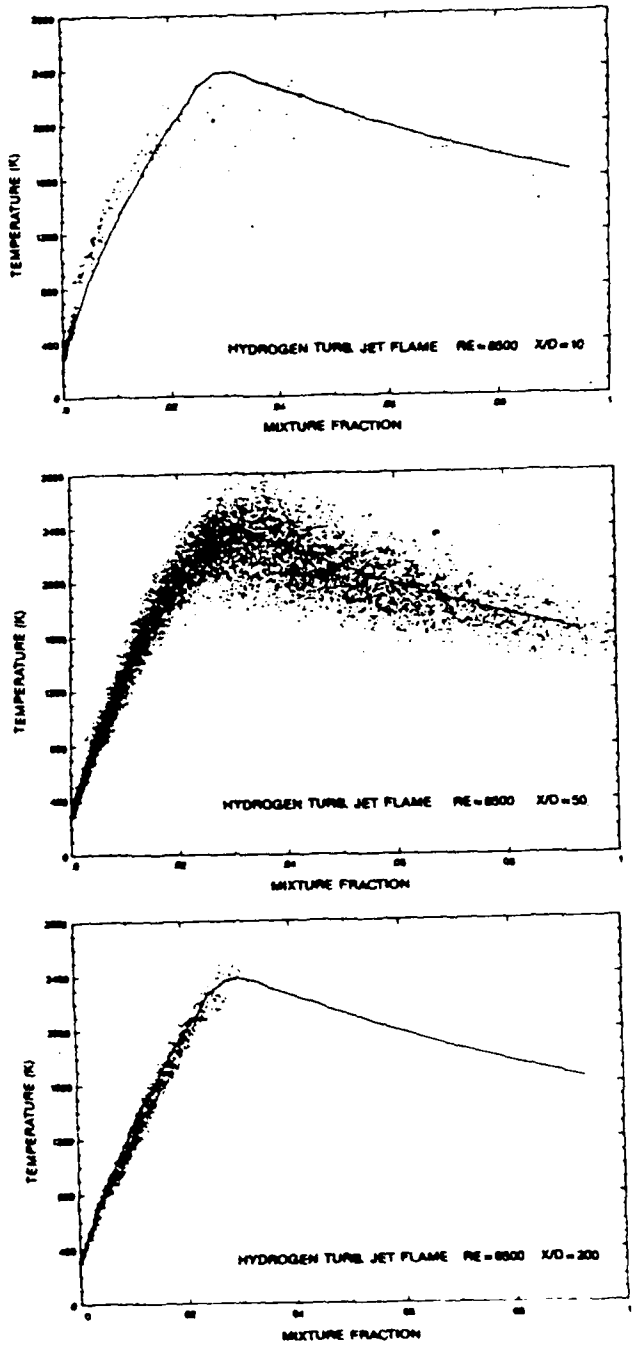

Figure 4 Instantaneous measurements of temperature and mixture fraction using pulsed-laser-Raman scattering from the H_2 turbulent jet-diffusion flame. Each of the ~30,000 points represents one time (2μs) and space (<0.1 mm^3) resolved measurement. Data from three axial positions (x/d = 10, 50 and 200) are shown. The solid line is the calculated relationship between temperature and mixture fraction in H_2-air flames under adiabatic equilibrium conditions.

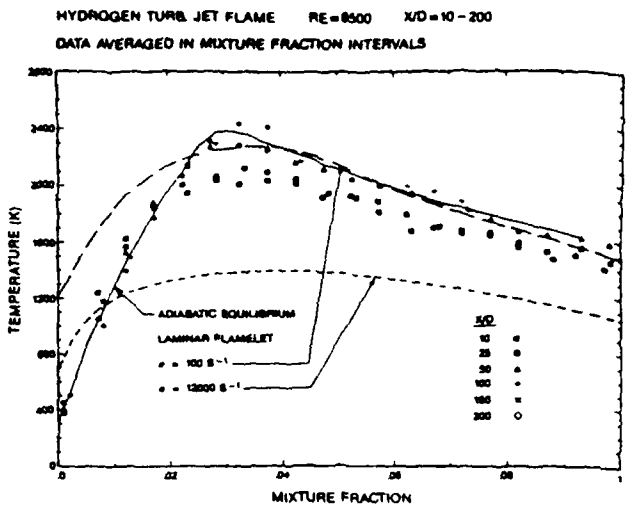

Figure 5 Data conditionally-averaged in mixture fraction intervals from the H_2 turbulent jet-diffusion flame at all six axial locations measured. The solid line is the same as in Figure 4. The dotted lines are those calculated by David et al.[9] for laminar opposed-flow H_2 diffusion flames under small stretch ($a \approx 100\ s^{-1}$) and near extinction ($a = 12{,}000\ s^{-1}$).

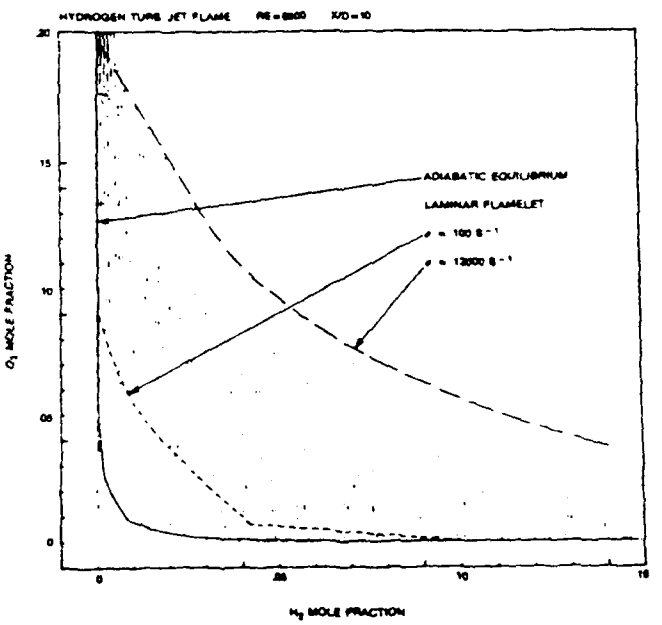

Figure 6 Instantaneous measurements of O_2 and H_2 mole fractions using pulsed-laser-Raman scattering from the H_2 turbulent jet-diffusion flame close to the fuel exit at x/d = 10 and 25. The solid and dashed curves are the same as in Figure 5.

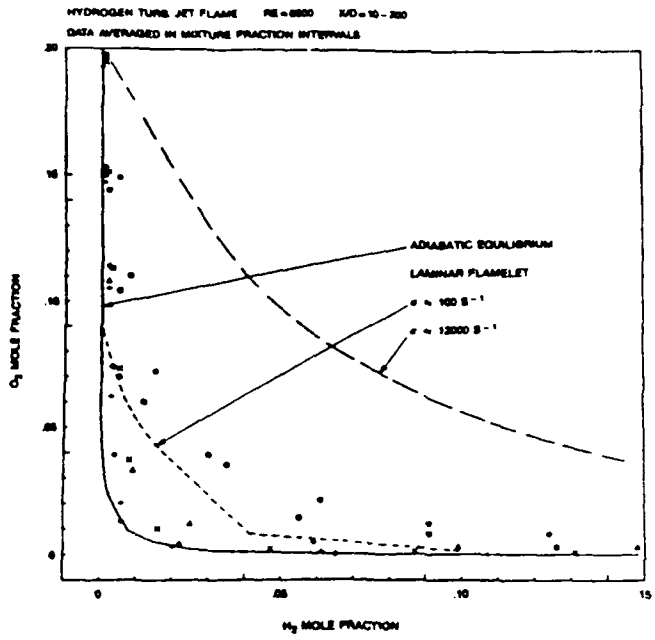

Figure 7 Data conditionally-averaged in mixture fraction intervals in the H_2 turbulent jet-diffusion flame showing the copresence of H_2 and O_2.

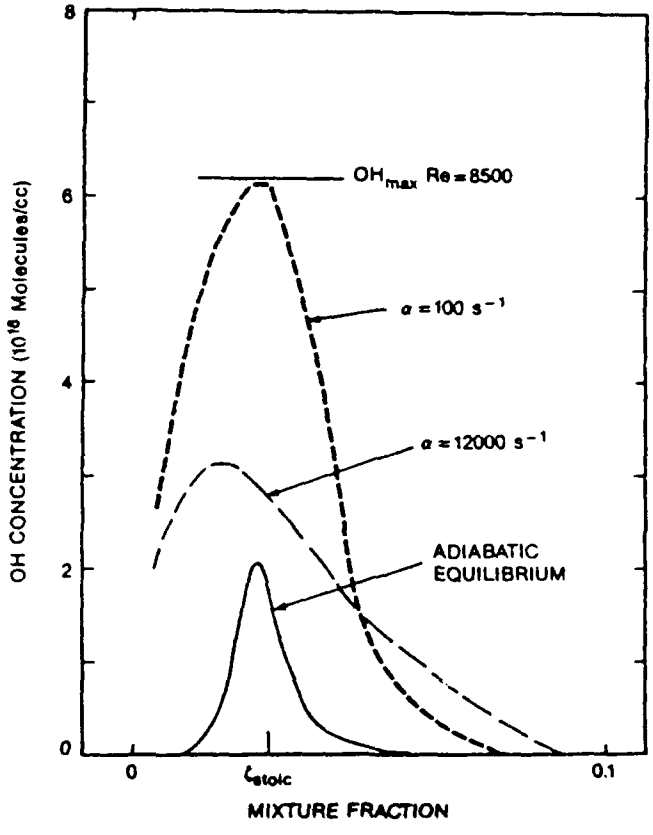

Figure 8 The OH concentrations versus mixture fraction calculated assuming adiabatic equilibrium (solid curve) and calculated by David et al.[9] for laminar-opposed flow H_2 diffusion flames under small stretch (α = 100 s^{-1}) and near extinction (α = 12,000 s^{-1}). The maximum instantaneous OH concentration measured by laser-saturated fluorescence in the Re = 8500 H_2 turbulent jet-diffusion flame is shown by the solid horizontal line.

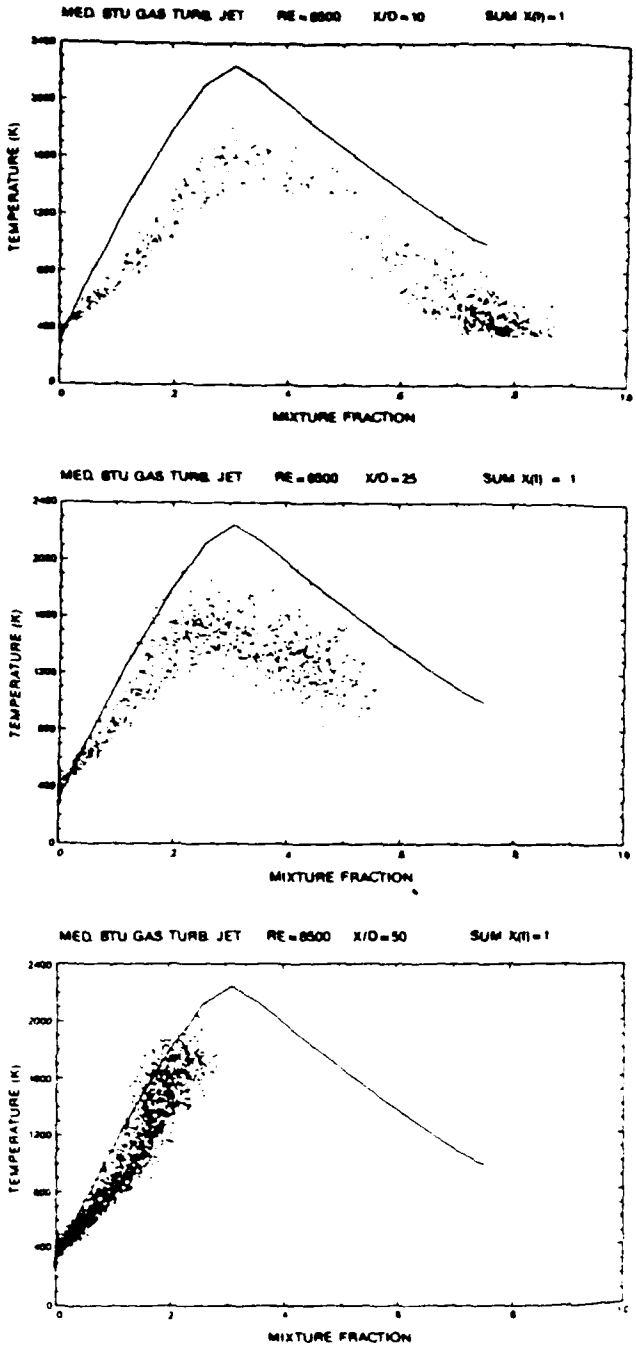

Figure 9 Instantaneous pulsed-Raman measurements of temperature and mixture fraction from a turbulent jet-diffusion flame with 40%CO/30%H_2/30%N_2 fuel. Temperatures were measured assuming the ideal gas law from the sum of the mole fractions of all major species measured by their respective Stokes vibrational Raman intensities. The solid line is the calculated adiabatic equilibrium curve for the CO/H_2/N_2 fuel mixture.

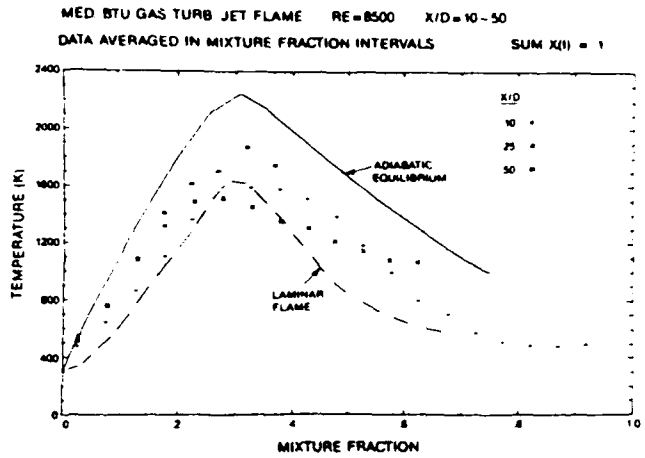

Figure 10 Conditionally-averaged Raman measurements of temperature and mixture fraction in the turbulent $CO/H_2/N_2$ jet diffusion flame at x/d = 10, 25 and 50 (data points) and from the laminar opposed-flow diffusion flame with the same fuel (dotted line).

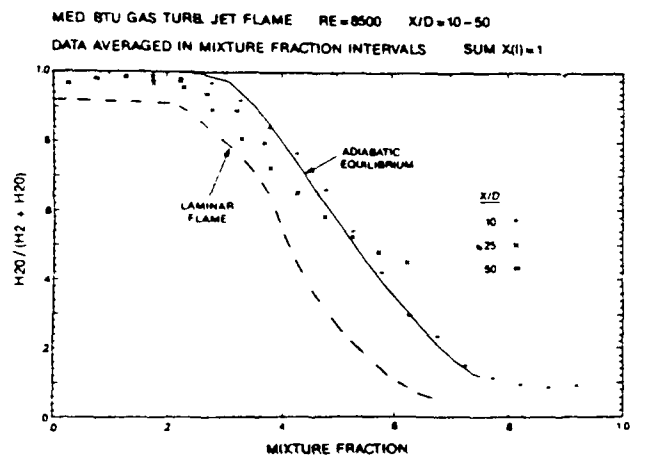

Figure 11 Conditionally-averaged Raman measurements of the conversion of H_2 versus mixture fraction in the turbulent jet-diffusion flame and laminar opposed-flow diffusion flame with $CO/H_2/N_2$ fuel. Symbols are the same as in Figure 10.

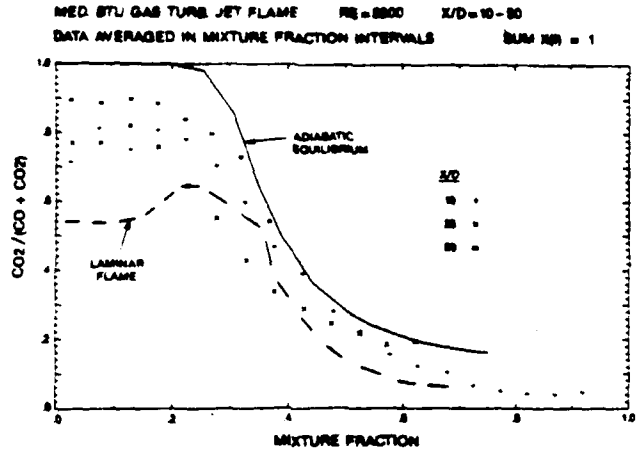

Figure 12 Conditionally-averaged Raman measurements of the conversion of CO versus mixture fraction in the turbulent jet diffusion flame and laminar opposed-flow diffusion flame with $CO/H_2/N_2$ fuel. Symbols are the same as in Figure 10.

Approved for public release;
distribution unlimited.

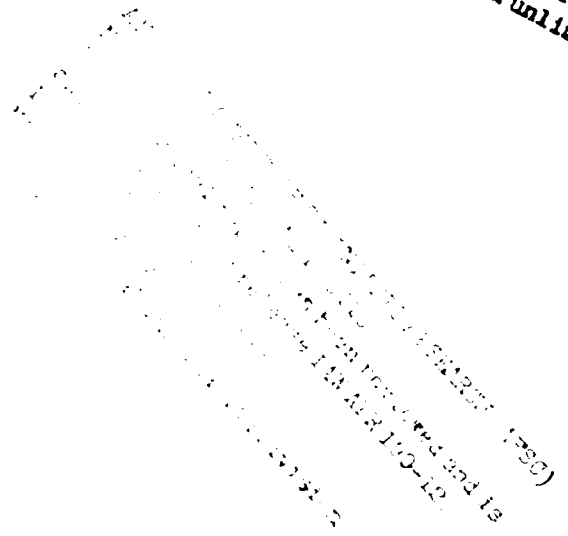

END

1-87

DTIC